Biophysical Journal Volume 100 June 2011 2576–2585

Coupling Active Hair Bundle Mechanics, Fast Adaptation, and Somatic Motility in a Cochlear Model

Julien Meaud[†*] and Karl Grosh[†‡]
[†]Department of Mechanical Engineering and [‡]Department of Biomedical Engineering, University of Michigan, Ann Arbor, Michigan

ABSTRACT One of the central questions in the biophysics of the mammalian cochlea is determining the contributions of the two active processes, prestin-based somatic motility and hair bundle (HB) motility, to cochlear amplification. HB force generation is linked to fast adaptation of the transduction current via a calcium-dependent process and somatic force generation is driven by the depolarization caused by the transduction current. In this article, we construct a global mechanical-electrical-acoustical mathematical model of the cochlea based on a three-dimensional fluid representation. The global cochlear model is coupled to linearizations of nonlinear somatic motility and HB activity as well as to the micromechanics of the passive structural and electrical elements of the cochlea. We find that the active HB force alone is not sufficient to power high frequency cochlear amplification. However, somatic motility can overcome resistor-capacitor filtering by the basolateral membrane and deliver sufficient mechanical energy for amplification at basal locations. The results suggest a new theory for high frequency active cochlear mechanics, in which fast adaptation controls the transduction channel sensitivity and thereby the magnitude of the energy delivered by somatic motility.

INTRODUCTION

The mammalian inner ear exhibits both remarkable frequency selectivity and sensitivity to low intensity acoustic stimuli. The dynamic range of hearing is expanded by a compressive nonlinearity of the cochlea's response to sound. In addition, a healthy cochlea can sometimes spontaneously emit sound (otoacoustic emissions) (1). These characteristics can be explained by a nonlinear active mechanism, called the cochlear amplifier (2), that can alter the response of the system to low-level stimuli and is necessary for normal hearing. A principal problem in cochlear biophysics is determining the relative contributions of outer hair cell (OHC) somatic motility (due to the action of prestin) and OHC hair bundle (HB) motility (linked to adaptation of the transduction current (3,4)) to amplification (5,6).

According to the most widely accepted theory, the active process in the mammalian cochlea is driven by the conversion of electrical to mechanical energy by a voltage-sensitive transmembrane protein, prestin (7), in the OHC lateral wall (e.g., see (8)). When the HBs of the OHCs are deflected due to vibrations in the organ of Corti (OoC), the HB transduction channel opens and the current depolarizes the OHC. The resulting transmembrane potential produces a force (9) at high frequencies (10). Recent experiments that alter force production by prestin, either by perfusion with salicylate (11) or genetic mutation (12,13), have proven that prestin-based motility is necessary for normal cochlear function. The main criticism of the somatic force generation hypothesis is that the low-pass filtering due to the OHC basolateral membrane electrical impedance reduces the potential associated with an HB-generated current so that the somatic force is unable to amplify the motion of the structures of the OoC (14). However, we have previously predicted (15,16) that the OHC transmembrane potential arising from acoustic stimulation is sufficient for somatic motility alone to provide high frequency amplification. In this study, we examine the role of HB adaptation on the active process at high frequencies and determine whether this prediction still holds once HB forcing is included into the mathematical model.

Of course, the presence of HBs is also requisite as the channels must be activated (i.e., opened) for the time-varying transduction current to flow. Once opened, calcium-mediated fast adaptation will occur. Over that past five years, fast adaptation (17–20) and force production (19,20) on a submillisecond timescale have been reported in mammalian HBs. Slow adaptation and force production (20) are also observed; however, this modality likely does not play a direct role in cycle-by-cycle amplification. From the measurements, it is now reasonable to assume that HBs can generate forces on a timescale commensurate with high frequency sound, but it is not clear that this force has sufficient authority to influence the response of the basilar membrane (BM) or other cochlear structures. Different models, based on the gating spring model of transduction (21), have been developed to predict the active HB dynamics. Fast adaptation has been modeled by different mechanisms that promote channel reclosure or reduce tension in the gating spring through the binding of calcium to some moiety in the channel (3,22,23). The theoretical analysis of Sul and Iwasa (24) of an individual HB, calls into question whether HBs can act as the sole source of amplification at high frequencies, as the HB cannot produce enough mechanical energy to overcome the viscous

Submitted November 22, 2010, and accepted for publication April 27, 2011.
*Correspondence: jmeaud@umich.edu
Editor: Andrew McCulloch.

0006-3495/11/06/2576/10 $2.00
doi: 10.1016/j.bpj.2011.04.049

damping in the subtectorial gap in mammals. We reexamine this result in the context of a complete cochlear model.

Because of the difficulty in isolating the effect of somatic motility and HB motility in a conclusive in vivo experiment, theoretical models have been used to establish the contributions of the two active mechanisms to cochlear amplification, as described in recent articles (5,25–27). In Reichenbach and Hudspeth (25) somatic motility was not incorporated at the base of the cochlea because the authors claim that somatic motility is negligible at high frequencies. Ó Maoiléidigh and Jülicher (26) and Nam and Fettiplace (27) analyzed the effect of the two active processes using realistic models of the OoC but restricted their studies to one cross section (i.e., uniform properties longitudinally) and did not include fluid loading and fluid longitudinal coupling. In a previous article, we included a simple phenomenological model for the added energy due to HB motility in our macroscopic cochlear model (5). Although these models provide insight into the possible contributions of the two active modalities, they are incomplete in at least one key aspect, and therefore their predictions are of limited generality. More-comprehensive models of the cochlea are needed, and must include the micromechanics of the OoC and OHC motility as well as macroscopic contributions such as fluid loading and electrical conductivity. The predictions of the force, voltage, current, and mechanical power generated by motility enable specific comparisons to in vitro and in vivo cellular level measurements to test the model.

In contrast to the high sensitivity and sharp tuning of the BM response to high frequency stimulation, limited positive or negative feedback and poor tuning have been observed at the apex of the cochlea in response to low frequency sounds (reviewed in Robles and Ruggero (1)). Moreover, the stiffness gradient of the BM might not be able to explain the frequency range of hearing (28). Therefore, different mechanisms have been proposed to explain the differences between apical and basal cochlear mechanics and to extend the range of hearing (25,29–31). Coiling of the cochlear ducts could have an effect on the low frequency response and on the micromechanics of the organ of Corti (29). A ratchet mechanism coupling HB and somatic motility has been proposed as the biophysical basis for low-frequency hearing by Reichenbach and Hudspeth (25). Moreover, the deflection of the HB of the OHC might involve the squeezing of the fluid in the subtectorial space at low frequencies (30). Finally, detailed modeling of the unloaded BM indicates that its mode of deformation might be different at low frequencies (31). These effects, which may be important at the apex, are not included in our model because our focus is on high frequency mechanics in the basal portion of the cochlea.

In this article, we use a mathematical model to predict the effect of coupling fast adaptation, active HB mechanics, and OHC somatic motility on the response of the cochlea. This model includes three-dimensional fluid effects, longitudinal electrical conduction, and a micromechanical model of the organ of Corti. The nonlinear dynamics of the HB, based on a six-state channel reclosure model of the HB (32), is linearized for small harmonic stimuli and then incorporated into our global model. The advantage of this approach is that we explicitly separate the contributions of each active modality and analyze their influence on the mechanics of the hearing organ, estimating, for instance, if forces are sufficient to modulate the BM response. Moreover, we model the effect of introducing pharmacological agents (such as salicylate (11)) or varying ionic concentrations on the cochlear response.

METHODS

Active nonlinear HB model

We describe here the nonlinear model of the active HB dynamics used as a basis for the linearized HB model. As in Sul and Iwasa (24) and Choe et al. (32), fast adaptation is modeled by a reclosure mechanism. The slow adaptation motor is assumed to set the resting tension in the gating spring but not to affect the dynamics of the HB at the frequencies considered here. The six-state transduction channel model, with two calcium-binding sites, is similar to that presented by Choe et al. (32) and is described in Fig. S1 *a* in the Supporting Material. In this model, calcium binding of some moiety in the channel causes a reduction in the intrinsic energy difference between the closed and open states of the channel.

When an external force, F_{ext}, is applied to the HB, the differential equation governing the motion of the HB is given by

$$c_{hb}\frac{du_{hb}}{dt} + N\gamma t_{gs} + K_{sp}\left(u_{hb} - X_{sp}\right) = F_{ext}\,, \qquad (1)$$

where c_{hb} is the damping coefficient of the HB due to the viscous fluid, N is the number of transduction channels per HB, t_{gs} is the tension in each gating spring, γ is the geometrical gain factor relating HB motion to the tip link motion (3,21), K_{sp} is the stiffness of the stereocilia pivot, X_{sp} is a constant, and u_{hb} is the displacement at the tip of the HB, in a direction perpendicular to the length of the HB ($u_{hb} = 0$ corresponds to equilibrium). The tension in each gating spring is given by

$$t_{gs} = k_{gs}(x_{hb} - x_a - P_0 d), \qquad (2)$$

where k_{gs} is the gating spring stiffness, d is the gating swing, P_0 is the open probability of the transduction channel, x_a is the position (assumed to be a constant) of the slow adaptation motor in the tip link direction (33), and x_{hb} is the displacement of the HB in the tip link direction ($x_{hb} = \gamma u_{hb}$).

As in Beurg et al. (20) and Choe et al. (32), the two binding sites are assumed to have the same affinity to calcium (modeled by the dissociation constant in the open state $K^o{}_D$, and in the closed state, $K^c{}_D$) and calcium binding coefficient (denoted as $K^o{}_B$ in the open state and $K^c{}_B$ in the closed state). The calcium concentration is denoted as $C^o{}_{fa}$ and $C^c{}_{fa}$ for the open and closed states, respectively.

The energy difference between the open and closed states of the channel is given by

$$\Delta E = f_{gs}x_{hb} + \Delta E_0 - n_{Ca}\epsilon_{Ca}, \qquad (3)$$

where f_{gs} is the single-channel gating force in the tip link direction (f_{gs} is given by $f_{gs} = k_{gs}\,d$ and is chosen to be 10 pN (20,24)) and ΔE_0 is the energy difference between the unbound open and closed states of the channel at $x_{hb} = 0$ (due to the resting tension of the gating spring and to the intrinsic energy difference between the open and closed states of the channel), n_{Ca} is the number of calcium ions bound to the channel ($n_{Ca} = 0$, 1, or 2), and ε_{Ca} is a constant energy that represents the reduction in the intrinsic energy

difference of the channel due to calcium binding. Based on a thermodynamic analysis of the HB (24), the constant is given by the ratio of the dissociation constants, where $\epsilon_{Ca} = k_B T\, ln(K_D^o/K_D^c)$. The equations for the rates of calcium binding and unbinding and of channel opening and closing are detailed in the Supporting Material.

Passive HB model

The passive HB is modeled by a two-state channel (shown in Fig. S1 *b*), with only states 1 (closed) and 2 (open). In this model, the HB performs forward transduction but does not convert chemical to mechanical energy. The intrinsic barrier and resting open probability $P_0^{\,s}$ are assumed to be the same as in the active HB model. This requires the energy difference between the open and closed state, $\Delta E_0^{\,NA}$, to have a different value than in the active HB model (ΔE_0), as seen in Table S3 in the Supporting Material.

Linearized HB model

Let P_i (where $i = 1,\ldots,6$) represent the probability of the channel to be in state i, as shown in Fig. S1 *a*. Using the additional constraint $\sum_{i=1}^{6} P_i = 1$, the equations of the kinetic scheme of the six-state channel (Fig. S1 *a*) can be reduced to the nonsingular matricial form

$$\frac{d\mathbf{P}}{dt} = \mathbf{A}\left(\frac{f_{gs}\, x_{hb}}{2k_B T}\right)\mathbf{P} + \mathbf{B}, \tag{4}$$

where $\mathbf{P}$ is the vector formed by the probabilities of each state $\mathbf{P} = [P_1,P_2,P_3,P_4,P_5]$; $\mathbf{A}$ is a 5×5 matrix that is a function of the HB deflection, $x_{hb;}$ k_B is Boltzmann's constant; T is the temperature; and $\mathbf{B}$ is a constant vector. The vector of resting probabilities for $x^s_{hb} = 0$, $\mathbf{P^s}$, is found by solving $\mathbf{A}\ (0)\ \mathbf{P^s} + \mathbf{B} = 0$.

Using the same approach as in Sul and Iwasa (24), the nonlinear differential equations governing the dynamics of the HB (Eqs. 1 and 4) are consistently linearized around the stationary point (x^s_{hb}, $\mathbf{P^s}$) for small harmonic perturbations δF_{ext}. We assume a time dependence $e^{-i\omega t}$, where ω is the radian frequency. Equation 4 becomes

$$\begin{aligned}\delta\mathbf{P} = &-\frac{f_{gs}}{2k_B T}\left(\mathbf{A}\left(\frac{f_{gs}x_{hb}}{2k_B T}\right)\Big|_{x_{hb}=x^s_{hb}} + i\omega\mathbf{I}\right)^{-1}\\ &\times\ \mathbf{A}'\left(\frac{f_{gs}x_{hb}}{2k_B T}\right)\Big|_{x_{hb}=x^s_{hb}} \mathbf{P^s}\delta x_{hb},\end{aligned} \tag{5}$$

where $\mathbf{I}$ denotes the 5×5 identity matrix and $\mathbf{A}'$ is the derivative of $\mathbf{A}$ with respect to its argument. The change in the open probability is given by $\delta P_0 = \delta P_2 + \delta P_3 + \delta P_4$.

A description of the optimization of the parameters of the transduction channel model can be found in the Supporting Material. The values for the physical parameters of the HB are given in Table S1.

Mechanical-electrical-acoustical model of the cochlea

The linearized model of the HB is implemented in a three-dimensional finite element model of the cochlea, described in Ramamoorthy et al. (15) and Meaud and Grosh (16). As shown in Fig. 1, the model includes the fluid (modeled as inviscid and incompressible), the structure (with a model for the organ of Corti represented in Fig. 1 *a* that includes the BM, and a bending and a shearing mode for the tectorial membrane (TM)), and electrical degrees of freedom (to represent the potentials in the scalae of the cochlea). The structural and electrical degrees of freedom are coupled via the somatic motility and HB mechanoelectrical transduction (as will be described in the next sections and as shown in Fig. 1 *b*). The model includes damping in the governing equations for the BM and TM to account for viscous losses in the subtectorial space, in the TM and in the BM. As in Ramamoorthy et al. (15) and Meaud and Grosh (16), the parameters of the cochlear model are based on experimentally measured properties for the guinea pig, when available (see Table S5 and Table S6).

OHC electromotility and mechanoelectrical coupling

As in Ramamoorthy et al. (15), Meaud and Grosh (16), and Tolomeo and Steele (34), the response of each individual OHC is described by linearized piezoelectric-like expressions (see Fig. 1 *b*) relating the OHC deformation, u_{ohc}^{comp}, and fluctuating part of the transmembrane voltage, $\Delta\phi_{ohc}$, to the OHC force, $F_{ohc,}$ and current, $I_{ohc,}$ as

$$\begin{aligned}F_{ohc} &= K_{ohc}u_{ohc}^{comp} + \epsilon_3\Delta\phi_{ohc}\\ I_{ohc} &= \frac{\Delta\phi_{ohc}}{Z_m} + i\omega\epsilon_3 u_{ohc}^{comp}\end{aligned}, \tag{6}$$

where K_{ohc} is the OHC stiffness, ε_3 is the electromechanical coupling coefficient, and Z_m is the basolateral impedance of the OHC. The mechanical energy generated by somatic electromotility per OHC per cycle is given by

$$E_{som} = -\pi Im[\epsilon_3\Delta\phi_{ohc} \times (u_{ohc}^{comp})^*], \tag{7}$$

where * denotes the complex conjugate and $Im[\cdot]$ the imaginary part of a complex number. As in Meaud and Grosh (16), the simulations are performed with an electromechanical coefficient, ε_3, of -1.08×10^{-10} N/mV at the 17-kHz best place (BP).

RESULTS

The HB mechano-electric transducer sensitivity and active HB force are related

In the nonlinear model of the HB, the active reclosure mechanism (see Methods and the Supporting Material) is responsible for the active HB mechanics and fast adaptation of the transduction current. Because the physiologically relevant displacements of the HB are small for low intensity acoustic stimulation, the linearized model for the HB dynamics described in Linearized HB Model, above, is used. Based on Eq. 5, the equations relating time harmonic oscillations of radian frequency in the HB force (for each individual HB), that is, δF_{hb}, transduction channel current, δi_0, and HB displacement, u_{hb}, are

$$\begin{aligned}\delta F_{hb} &= \left[K_{pass} - K_{act}(\omega)\right]u_{hb}\\ \delta i_0 &= G_a^{max}J(\omega)V^s u_{hb}\end{aligned}, \tag{8}$$

where K_{pass} is the passive HB stiffness (given by $K_{pass} = K_{sp} + N\gamma^2 k_{gs}$), $K_{act}(\omega)$ the complex active dynamic stiffness of the HB (due to gating compliance (3), and fast adaptation), $J(\omega)$ represents the sensitivity of the transduction channel to HB deflection, V^s is the resting potential across the HB, and G_a^{max} is the maximum saturating conductance of the entire HB. The values $J(\omega)$ and $K_{act}(\omega)$ are given by

$$J(\omega) = \frac{\gamma f_{gs}}{k_B T}TF(\omega), \tag{9}$$

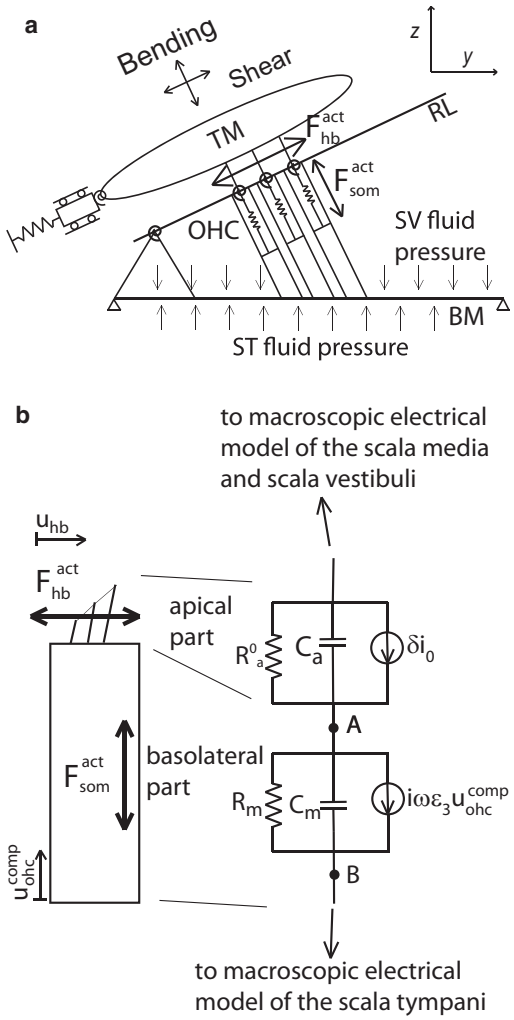

FIGURE 1 Coupling among cochlear macromechanics, organ of Corti kinematics, outer hair cell (OHC) somatic motility, and hair bundle (HB) activity in the model of the cochlea. (*a*) Model of the organ of Corti kinematics. As in Ramamoorthy et al. (15), the basolateral membrane (BM) deformation is modeled by a simply supported BM mode shape and the tympanic membrane (TM) by its shearing and bending modes. Different cross sections of the BM and TM are connected due to structural longitudinal coupling (16). The fluid in the scala vestibuli (SV) and scala tympani (ST) applies in a pressure on the BM. The fluid pressure in the SV and ST is coupled to the BM velocity via the linearized Euler relation. As shown in Eq. 6, each OHC soma is modeled by the superposition of a linear spring and of an active force along the length of the OHC, $F^{act}_{som} = \varepsilon_3 \Delta\phi_{ohc}$. Each HB is modeled by the superposition of a rotational spring (modeled by an equivalent linear spring with stiffness K_{pass}) and of an active force, $F^{act}_{hb} = -K_{act}(\omega)u_{hb}$ (see Eq. 8). The contributions from the three rows of OHC to the somatic and HB forces are added. (*b*) Coupling between the mechanical model of the OHC and its electrical model. The active somatic force (F^{act}_{som}), the active HB force (F^{act}_{hb}), the HB deflection (u_{hb}), and the OHC compression (u^{comp}_{ohc}), are coupled to the electrical domain. The apical part and basolateral parts of each OHC are modeled by an electrical circuit similar to Ramamoorthy et al. (15). The resting conductance of the HB, $1/R_a{}^0$, and capacitance, C_a, are in parallel with a current source δi_0 corresponding to the transduction current and proportional to the HB deflection, u_{hb}, as shown in Eq. 8. The basolateral part of the OHC includes the basolateral conductance, $1/R_m$, and capacitance, C_m, of the OHC, as well as a current source, $i\omega u^{comp}_{ohc}$, proportional to the OHC compression (see Eq. 6). The OHC depolarization, $\Delta\phi_{ohc}$, is the potential drop from point A to point B. The contributions from the three rows of OHC are added and integrated into a macroscopic model of the potentials in the scala media, scala tympani, and scala vestibuli that includes longitudinal cables to represent propagation of current along the length of the cochlea (15). HB activity affects the active HB force, $F_{hb}{}^{act}$, as well as the current source δi_0.

$$K_{act}(\omega) = \frac{N\gamma^2 f_{gs}^2}{k_B T} TF(\omega), \tag{10}$$

where $TF(\omega)$ is the nondimensional-complex-valued, frequency-dependent transduction channel filter (obtained by solving Eq. 5).

The mechanical energy generated by the HB per cycle depends on the imaginary part of the active stiffness as

$$E_{hb} = \pi Im[K_{act}(\omega)]|u_{hb}|^2, \tag{11}$$

where for this sign convention $E_{hb} > 0$ represents dissipation and $E_{hb} < 0$ generation. These relations reveal that HB energy generation (Eq. 11), the mechano-electric transducer (MET) sensitivity (given by $G_a^{max}\ J(\omega)V^s$), and the active HB force ($K_{act}(\omega)u_{hb}$), are related and depend on the same frequency-dependent filter, $TF(\omega)$. HB energy generation is proportional to f_{gs}^2 (as shown in Sul and Iwasa (24)). We highlight here that the MET sensitivity is proportional to $G_a^{max}V^s f_{gs}$, explicitly showing the linkage between MET sensitivity and HB forcing. The parameters of the transduction channel have been optimized to maximize the peak of the mechanical energy delivered by the HB. The HB parameters are then adjusted so that the transduction channel filter varies spatially and is tuned to a frequency chosen to maximize the peak of the BM response to acoustic stimulation (see the Supporting Material).

The transduction channel is a poorly tuned bandpass filter and the dynamics of fast adaptation reduces the MET channel sensitivity

The magnitude and phase of the transduction channel filter, $TF(\omega)$, are plotted as a function of frequency in Fig. 2, *a* and *b*, for an isolated HB at the 17-kHz best place (BP). In a model without adaptation (see Methods), the transduction channel filter is a low-pass filter with a characteristic frequency (CF) of 224 kHz, limited by kinetics of channel activation. When the fast adaptation mechanism is included, $TF(\omega)$ is a poorly tuned bandpass filter, with a barely discernible peak at 30.0 kHz. At CF, $|TF(\omega)|$ and hence the MET sensitivity (see Eqs. 8 and 9), are ~25% lower with adaptation than without adaptation. The phase of $TF(\omega)$ is $\sim -2^\circ$ so that the MET current leads the HB displacement, but only by a small amount. The broad tuning of the transduction filter is also manifest in the real part of the active HB stiffness, $K_{act}(\omega)$, as shown in Fig. 2 *c*. The passive bundle stiffness

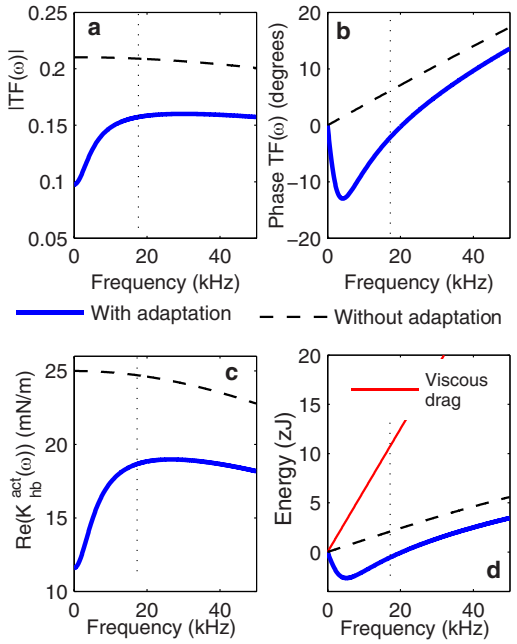

FIGURE 2 For a single isolated HB at the 17-kHz CF location, predictions of the transduction channel filter function, active stiffness, and energy generation are plotted versus frequency. These results vary spatially with frequency in a way described in Fig. S1. (*Vertical dots*) The CF. (*Thick solid line*) Predictions with fast adaptation and channel activation included in the model. (*Dashed line*) Results with only channel activation included. (*a*) Magnitude and (*b*) phase of the transduction channel filter, $TF(\omega)$ (defined by Eq. 9) which relates the MET current to HB displacement. (*c*) Real part of the active HB stiffness, K_{act} (ω). (*d*) Mechanical energy delivered per cycle by the HB (positive is dissipation, negative generation) for a 0.5-nm HB displacement. (*Thin solid line*) Energy dissipated by viscous drag in the subtectorial space.

(0.16 N/m at this location) is reduced only by 10% by the active stiffness.

Energy dissipation and generation by the effects of HB fast adaptation and channel activation are small

The mechanical energy generated by the HB as computed from Eq. 11 is shown in Fig. 2 *d* for a HB located at the 17 kHz BP. As in Sul and Iwasa (24), the magnitude of the energy dissipated or generated by the HB is predicted to be much smaller than the energy dissipated by viscous drag of the HB through the surrounding fluid, except at the lowest frequencies (<~10 kHz). The model without fast adaptation predicts that the HB dissipates mechanical energy over all frequencies. With fast adaptation, the HB delivers mechanical energy up to 20.4 kHz, with a peak at 5.2 kHz. At this frequency, the HB delivers more energy than dissipated by viscous drag. At frequencies above 20.4 kHz, the HB dissipates energy, but the amount of energy dissipated is small, more than one-order-of-magnitude less than viscous drag at CF, for instance.

A complete cochlear model including somatic motility and HB activity predicts the BM response to low intensity sound stimulation

The response of the BM to low intensity acoustic stimulation is simulated using a macroscopic mathematical model of the cochlea described in Fig. 1 that includes HB mechanoelectrical transduction and any combination of somatic motility (see Methods) and HB activity (fast adaptation and HB motility, modeled by Eq. 8). The predicted frequency dependence of the normalized BM displacement at the 17-kHz BP is shown in Fig. 3. The passive model of the BM response (without somatic motility or HB activity) exhibits a broad peak, as observed in measurements at high intensity or postmortem (35). With HB activity and somatic motility, the BM response approximately matches the sensitivity (with a 34 dB gain relative to a passive model), tuning (with a mechanical quality factor, Q_{10dB}, of 6.1 vs. 6.5 in the experiment), and peak frequency (~17 kHz) of the experimental response to low intensity acoustic input (35).

If somatic motility is included in the model but HB activity is not included, the model predicts a higher gain of the BM and a lower peak frequency. The presence of fast adaptation reduces the MET sensitivity (Fig. 2 *a*), which makes the system with somatic motility and HB activity less

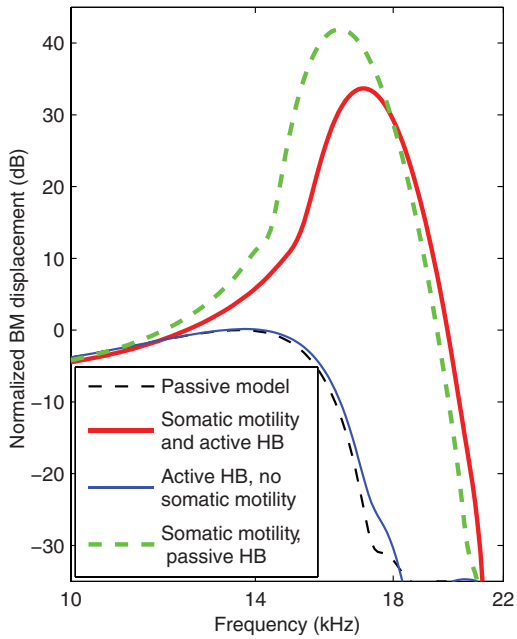

FIGURE 3 BM response to acoustic stimulus for three different cochlear models. Displacement of the BM in dB normalized to the maximum passive response due to acoustic stimulation at the 17-kHz best place. (*Thick solid line*) Prediction with somatic motility and HB activity (fast adaptation and active HB mechanics). (*Thick dashed line*) Prediction of a passive model. (*Thin solid line*) Theoretical prediction of HB activity only without somatic motility. (*Thin dashed line*) Prediction of a model with somatic motility and without HB activity.

sensitive and more stable than in a model with somatic motility and a passive HB. However, when HB activity is included and somatic motility is not included, the response reverts nearly to that of a passive model. The response of the BM as well of the shearing and bending modes of the TM at different longitudinal locations is shown in Fig. S4. At locations <~1.2 cm from the base of the cochlea, the fully active model (with somatic motility and HB activity) predicts qualitatively similar responses compared to Fig. 3.

Somatic motility, not HB motility, amplifies motion for frequencies near CF

When we speak of energy generation, we mean net conversion to mechanical energy from some other form of energy on a cycle-by-cycle basis. Somatic motility can convert electrical energy (in the form of the resting endocochlear potential) to mechanical energy (e.g., Ramamoorthy et al. (15)) in a nearly reciprocal fashion (36) while HB activity can transfer chemical energy to mechanical energy during the binding process (24,32). The results for an individual HB presented in Fig. 2 *d* are now revisited by making predictions in a global cochlear model. The mechanical energy delivered per cycle by the somatic force and the HB force is plotted as a function of frequency in Fig. 4 for a 0.5-nm BM displacement. For this location, the upper limit of energy generation derived from somatic motility is 21.7 kHz (this limit depends on the micromechanics of the OoC) whereas that for HB motility is 20.4 kHz (as in Fig. 2 *d*, this limit depends on the kinetics of the MET channel). Hence, both motilities deliver mechanical energy at CF. Note that the peak of energy generation for HB motility (as well as somatic motility) corresponds to the CF; this peak is due to the peak in the HB deflection at CF. However, the energy delivered by the HB is about two orders of magnitude lower than the energy delivered by the OHC soma at CF. From 11.1 kHz to 19.0 kHz, somatic motility delivers more energy than the energy dissipated in the organ of Corti and subtectorial space.

The gain of the BM response to acoustic stimulation depends on the somatic electromechanical coupling coefficient and on the calcium concentration

We varied the electromechanical coupling coefficient (ε_3 in Eq. 6) so as to determine the effect of a small reduction in prestin activity, as might be induced by intracellular perfusion of salicylate (11). In Fig. 5, the BM gain in response to low intensity acoustic stimulation is reduced by 6.1 dB when ε_3 is reduced by 10%, similar to reductions seen in salicylate perfusion experiments. The procedure used to compute the effect of calcium on the transduction channel is described in the Supporting Material. An increase of the calcium concentration at the fast adaptation site (when the channel is open), C^o_{fa}, by 10%, results in a 2.3-dB reduction in the gain through a reduction of the amplitude of $TF(\omega)$. Alterations of the calcium concentration can be induced by disturbance of endolymph calcium homeostasis (for example in Meniere's disease (37)) or exposure to loud sounds (38), although the relation between these conditions and the calcium concentration is less clear than for the effect of salicylate on somatic electromotility.

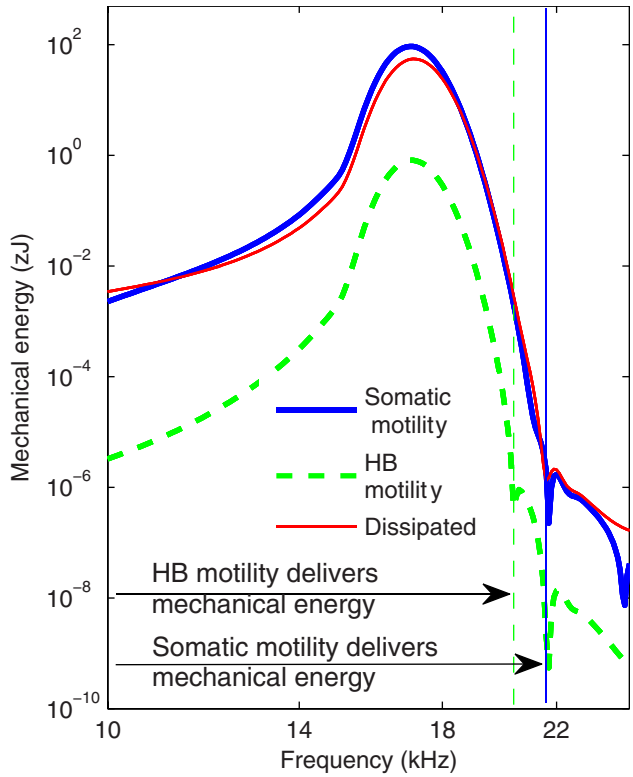

FIGURE 4 Energetics of active processes and dissipation. (*Thick solid line*) Magnitude of the mechanical energy generated by somatic electromotility per cycle for a 0.5-nm BM displacement. (*Thick dashed line*) Magnitude of the mechanical energy generated by HB activity. The sign change in energy gives the boundary between generation and dissipation; the active processes generate mechanical energy on the left of the vertical lines (as indicated by the *arrows*). (*Thin solid line*) Mechanical energy dissipated by viscous drag in the subtectorial space and by viscous damping in the TM and BM (see the Supporting Material).

Sensitivity of the model predictions to the HB parameters

The influence of the parameters of the HB (both the transduction channel properties and the HB stiffness) on the predictions of the BM response is analyzed in Fig. 6 (the effect of other parameters was studied in Ramamoorthy et al. (15) and Meaud and Grosh (16)). As the single-channel gating force, f_{gs}, is increased, the value of the CF does not change but the BM becomes more sensitive close to the CF (an increase of 10% increases the BM gain by 8.0 dB; see Fig. 6 *a*) because of the increase in the energy

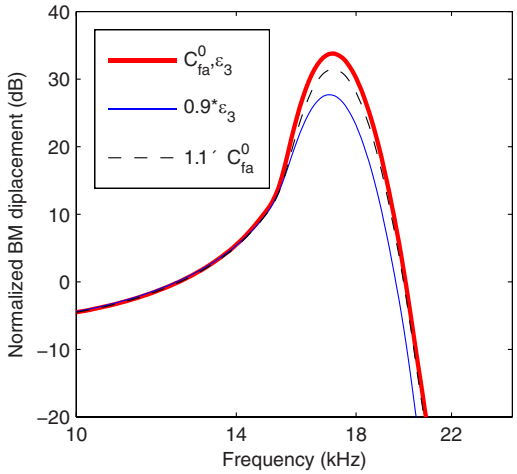

FIGURE 5 Effect of changes in the OHC somatic electromechanical coupling coefficient, ε_3, and in the endolymphatic calcium concentration, C_{fa}^o, on the predictions of the BM response to acoustic stimulation. The normalized BM gain is plotted as a function of frequency. (*Thick solid line*) Initial values for ε_3 and C_{fa}^o. (*Thin solid line*) C_{fa}^o is increased by 10%. (*Thin dashed line*) ε_3 is reduced by 10%.

delivered by HB motility (proportional to f_{gs}^2) and in the transduction current sensitivity (proportional to f_{gs}). The value of the maximum saturating conductance of the HB, G_a^{max}, has a similar (but not as pronounced) effect as f_{gs}, because G_a^{max} only affects the value of the transduction current. An increase of 10% of G_a^{max} increases the gain by 6.1 dB.

The effect of the value of the passive HB stiffness, K_{st}, is shown in Fig. 6 *c*.

As the passive HB stiffness is reduced, the peak of the BM response shifts to a lower frequency and has a higher magnitude. In the model, the most important factor controlling the CF of the BM (see Fig. S4) is the passive resonance of the uncoupled TM shear mode (the resonant frequency is given by $\sqrt{K_{tms}+3K_{st}/M_{tms}}$, where K_{tms} is the TM stiffness, M_{tms} is the TM shearing mass, and 3 is the number of HB per cross section). Therefore, as in the previous model of the cochlea (that did not include the active HB dynamics (15)), a reduction in the HB stiffness induces a reduction in the CF. The CF depends weakly on the peak frequency of the transduction channel filter, $TF(\omega)$, and we denote this peak frequency as F_{peak} (see the Supporting Material for more discussion on F_{peak}). In Fig. 6 *d*, we show that a 50% change in F_{peak} changes the CF by only a few percent.

DISCUSSION

In our model, we can explore a variety of ways for HB and somatic force generation and HB filtering to alter the mechanics and response of the cochlea. At the outset, we envisioned several potential scenarios for their interaction at high frequencies, including some sort of synergistic amplification by both processes. We found a very different

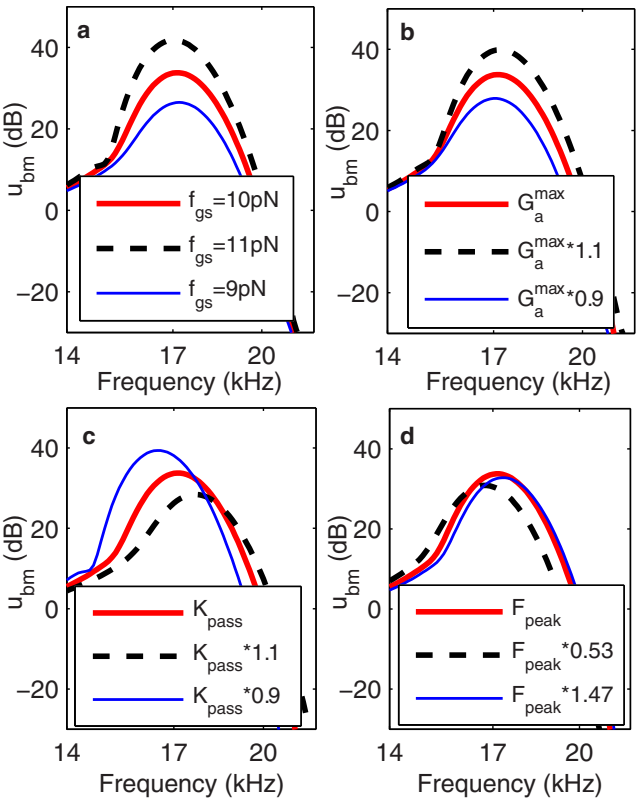

FIGURE 6 Sensitivity of the BM response to acoustic stimulation to the changes in the parameters of the HB. The normalized BM displacement, in dB, is plotted as a function of frequency at the 17-kHz best place. (*a*) Effect of changing the value of the single-channel gating force, f_{gs}. (*b*) Effect of changing the maximum saturating conductance of the HB, G_a^{max}. (*c*) Effect of changing the passive hair bundle stiffness, K_{pass}. (*d*) Effect of changing the peak frequency of the transduction channel filter, F_{peak}.

cooperation between the two modalities. Somatic motility provides the amplification at CF. Fast adaptation reduces the MET channel sensitivity and controls the magnitude of the energy delivered by somatic motility. HB amplification somewhat ameliorates the dissipative effects of channel gating, but neither the added energy nor the amount of dissipation are significant compared to dissipation by the HB moving through the fluid at high frequencies (see Fig. 2 *d*). Our simulations (see Fig. 4) confirmed the analysis that the energy generated per cycle by an isolated HB was not sufficient to influence high frequency global cochlear mechanics.

Resistor-capacitor filtering of the OHC transmembrane voltage does not preclude somatic motility from acting as the cochlear amplifier

Our results show that somatic motility can be the underlying source of high frequency mammalian cochlear amplification despite low-pass filtering of the transducer currents by the basolateral membrane of the OHC. In our model, the cutoff frequency of an isolated OHC is 280 Hz at the 17 kHz BP.

At this location, in a sensitive cochlea, a sound input at 17 kHz of ~20-dB sound pressure level gives rise to a BM displacement of 0.5 nm (39). For such a displacement, we predict a transduction current of 1.17 nA and a transmembrane potential of 480 μV for an OHC at this location. There is strong evidence that these are physiologically realistic values. In our model, the value of the HB saturating conductance, G_a^{max}, is set to 140 nS at the 17 kHz BP. Using the in vitro hemicochlea preparation at room temperature, He et al. (40) measured a conductance of 34.7 nS for a basal HB in the adult gerbil hemicochlea. The experimental values must be corrected to account for in vivo conditions including a lower in vivo calcium concentration (a factor of 2 (40)), higher temperature (a factor of 1.6 assuming a Q_{10} at ~1.3 (17)), and potassium as opposed to the sodium-based endolymph for experiment (a factor of 1.25 (17)) for a fourfold increase of the conductance to a value of 138 nS (within 2% of the value we use).

The largest in vitro current measured by He et al. (40) is 2.4 nA. Using the same temperature and ionic corrections as above, along with a factor of 2 for a larger in vivo resting DC potential, our estimate of the largest current is 28 nA—larger than our theoretical estimate near threshold of 1.17 nA. Moving to a discussion of the voltage, we predict an OHC transmembrane potential that is higher than the only in vivo transmembrane measurements (41) at these frequencies. This is expected, as discussed in He et al. (40), Dallos (42), Russell and Kössl (43), and Fridberger et al. (44), because the microelectrode measurement underestimates the receptor potential due to the leak conductance around the electrode, the piercing of the OHC membrane (which may reduce the driving DC receptor potential), the loss of sensitivity due to the overall surgical preparation, and any mechanical constraints due to the microelectrode penetration. Extracellular potential measurements are less invasive and our prediction (177 μV for a 0.5-nm BM displacement) is in good agreement with the measurement-based estimate of Fridberger et al. (44) (~80 μV for a 0.3-nm BM displacement) for a cochlea in good physiological condition.

Our theoretical model predicts the response that would be measured in a pristine sensitive cochlea. Hence, the quantitative differences are reasonable in view of the differences between the model and measurement configurations. We show that a submillivolt transmembrane potential is converted to an active somatic force of 50 pN at CF (<1% of the in vitro maximal values of ~10 nN (45)), a force sufficient to provide for the 30–40 dB gain difference between sensitive and insensitive conditions in vivo.

To achieve a transduction current of 1.17 nA at the 17-kHz best place, two additional factors are of central importance:

First, an electromechanical resonance of the OoC-TM system, due to the interaction of the TM mass (46,47), the compliance and kinematic constraints of the structures of the OoC, and the active somatic force, magnifies the HB shearing motion and maintains the appropriate phase of the HB transducer current. This electromechanical resonance is responsible for the sharp tuning of not only the transduction current, but also of the BM motion. This tuning does not arise from an intrinsic tuning of somatic electromotility (which is not tuned (10)) and depends only weakly on HB filtering (which was shown here to be poorly tuned in Fig. 2 *a* and Fig. 6 *d*).

The second important factor is the longitudinal propagation of electrical current in the scalae and interstitial space. By artificially altering the numerical values of the fluid conductances in our model, we tested the effect of longitudinal propagation of current in the scalae and the interstitial space on our predictions. Including this conductance path provides for roughly 5 dB of additional gain in our model due to an increase in the transmembrane potential that drives somatic motility. Note that our conclusions about the role of somatic motility is different from Ospeck et al. (48), who found a limiting frequency for amplification of ~13 kHz; however, their analysis was based on the lower conductance of an apical HB of the neonatal mouse (49) and did not include a TM mass resonance and the longitudinal propagation of current.

Could HB motility be the amplifier?

In our model, the value for the single-channel gating force is in good agreement with experimentally derived values for the mammalian HB (20,33,50). We found that a higher single-channel gating force (>20 pN), such as used in Nam and Fettiplace (51) or Ó Maoiléidigh and Jülicher (26), and faster kinetics for adaptation, is needed for the active HB force to have a more prominent role in high frequency cochlear amplification. Such a value of f_{gs} would result in unrealistic transduction current and OHC potentials at threshold. The calcium-binding coefficients we use at the base of the cochlea are near the upper limit for a diffusion-limited reaction (52); it is unlikely that the kinetics can be much faster. Therefore, it does not appear that HB forcing is responsible for cochlear amplification at high frequencies.

For lower-frequency hearing, nearer the apex of the cochlea, HB forcing may play a more important role (which would be consistent with the measurements of Chan and Hudspeth (53) showing calcium-dependent amplification of OHC deflection in an in vitro preparation of an apical segment of the cochlea). In this region, the HB force is able to overcome viscous drag in the subtectorial space at frequencies relevant to apical cochlear mechanics (see Fig. S5). Continued system level and cellular level biophysical measurements along with fully nonlinear mathematical models are still needed to completely describe the response of the cochlea. In light of our small-signal modeling results, we conclude that, in the base of the mammalian cochlea, prestin-mediated somatic motility of outer hair cells is the mechanism by which stored electrical energy is converted into mechanical energy driving cochlear amplification and providing for acoustic compression so essential to normal hearing.

Experiments supporting and needed to test our theory

The predictions by the model of the BM and TM displacements as well as of the electrical degrees of freedom in response to high frequency acoustic stimulation can provide data for indirect test of our theory. As discussed above, the predictions of the BM displacement, and intracellular and extracellular OHC potentials, are reasonable. Moreover, the somatic-based amplification mechanism proposed here is consistent with measurements made with intracochlear perfusion of salicylate (11) or prestin-knockin mutation (13)—interventions known to disrupt the prestin-based transduction and reduce cochlear output (either in the BM gain or auditory thresholds) as in our model (Fig. 5).

In vivo measurements of the TM response to acoustic stimulation (using techniques such as those employed by Hong and Freeman (54) and Choudhury et al. (55)) could also serve to validate this cochlear model. Moreover, the parameters of the HB model that are critical for our predictions (particularly G_a^{max} and f_{gs}) could be refined if measurements of the HB response in more physiologically relevant conditions were available. A more direct test of our theory could be the extension of the preparation of Chan and Husdpeth (53) to a basal segment of the cochlea; the conclusions of a similar experiment in a high frequency location could be used to validate or challenge our theory.

SUPPORTING MATERIAL

Additional informational text, including six figures, six tables, and 27 equations, is available at http://www.biophysj.org/biophysj/supplemental/S0006-3495(11)00527-3.

This research was supported by National Institutes of Health NIH-NIDCD R01-04084.

REFERENCES

1. Robles, L., and M. A. Ruggero. 2001. Mechanics of the mammalian cochlea. *Physiol. Rev.* 81:1305–1352.
2. Davis, H. 1983. An active process in cochlear mechanics. *Hear. Res.* 9:79–90.
3. Howard, J., and A. J. Hudspeth. 1988. Compliance of the hair bundle associated with gating of mechanoelectrical transduction channels in the bullfrog's saccular hair cell. *Neuron.* 1:189–199.
4. Ricci, A. J., A. C. Crawford, and R. Fettiplace. 2000. Active hair bundle motion linked to fast transducer adaptation in auditory hair cells. *J. Neurosci.* 20:7131–7142.
5. Ashmore, J. F., P. Avan, …, B. Canlon. 2010. The remarkable cochlear amplifier. *Hear. Res.* 266:1–17.
6. Peng, A. W., and A. J. Ricci. 2011. Somatic motility and hair bundle mechanics: are both necessary for cochlear amplification? *Hear. Res.* 273:109–122.
7. Zheng, J., W. Shen, …, P. Dallos. 2000. Prestin is the motor protein of cochlear outer hair cells. *Nature.* 405:149–155.
8. Ashmore, J. 2008. Cochlear outer hair cell motility. *Physiol. Rev.* 88:173–210.
9. Brownell, W. E., C. R. Bader, …, Y. de Ribaupierre. 1985. Evoked mechanical responses of isolated cochlear outer hair cells. *Science.* 227:194–196.
10. Frank, G., W. Hemmert, and A. W. Gummer. 1999. Limiting dynamics of high-frequency electromechanical transduction of outer hair cells. *Proc. Natl. Acad. Sci. USA.* 96:4420–4425.
11. Santos-Sacchi, J., L. Song, …, A. L. Nuttall. 2006. Control of mammalian cochlear amplification by chloride anions. *J. Neurosci.* 26:3992–3998.
12. Liberman, M. C., J. Gao, …, J. Zuo. 2002. Prestin is required for electromotility of the outer hair cell and for the cochlear amplifier. *Nature.* 419:300–304.
13. Dallos, P., X. D. Wu, …, J. Zuo. 2008. Prestin-based outer hair cell motility is necessary for mammalian cochlear amplification. *Neuron.* 58:333–339.
14. Santos-Sacchi, J. 1992. On the frequency limit and phase of outer hair cell motility: effects of the membrane filter. *J. Neurosci.* 12:1906–1916.
15. Ramamoorthy, S., N. V. Deo, and K. Grosh. 2007. A mechano-electro-acoustical model for the cochlea: response to acoustic stimuli. *J. Acoust. Soc. Am.* 121:2758–2773.
16. Meaud, J., and K. Grosh. 2010. The effect of tectorial membrane and basilar membrane longitudinal coupling in cochlear mechanics. *J. Acoust. Soc. Am.* 127:1411–1421.
17. Kennedy, H. J., M. G. Evans, …, R. Fettiplace. 2003. Fast adaptation of mechanoelectrical transducer channels in mammalian cochlear hair cells. *Nat. Neurosci.* 6:832–836.
18. Ricci, A. J., H. J. Kennedy, …, R. Fettiplace. 2005. The transduction channel filter in auditory hair cells. *J. Neurosci.* 25:7831–7839.
19. Kennedy, H. J., A. C. Crawford, and R. Fettiplace. 2005. Force generation by mammalian hair bundles supports a role in cochlear amplification. *Nature.* 433:880–883.
20. Beurg, M., J. H. Nam, …, R. Fettiplace. 2008. The actions of calcium on hair bundle mechanics in mammalian cochlear hair cells. *Biophys. J.* 94:2639–2653.
21. Markin, V. S., and A. J. Hudspeth. 1995. Gating-spring models of mechanoelectrical transduction by hair cells of the internal ear. *Annu. Rev. Biophys. Biomol. Struct.* 24:59–83.
22. Wu, Y. C., A. J. Ricci, and R. Fettiplace. 1999. Two components of transducer adaptation in auditory hair cells. *J. Neurophysiol.* 82:2171–2181.
23. Martin, P., D. Bozovic, …, A. J. Hudspeth. 2003. Spontaneous oscillation by hair bundles of the bullfrog's sacculus. *J. Neurosci.* 23:4533–4548.
24. Sul, B., and K. H. Iwasa. 2009. Effectiveness of hair bundle motility as the cochlear amplifier. *Biophys. J.* 97:2653–2663.
25. Reichenbach, T., and A. J. Hudspeth. 2010. A ratchet mechanism for amplification in low-frequency mammalian hearing. *Proc. Natl. Acad. Sci. USA.* 107:4973–4978.
26. Ó Maoiléidigh, D., and F. Jülicher. 2010. The interplay between active hair bundle motility and electromotility in the cochlea. *J. Acoust. Soc. Am.* 128:1175–1190.
27. Nam, J. H., and R. Fettiplace. 2010. Force transmission in the organ of Corti micromachine. *Biophys. J.* 98:2813–2821.
28. Naidu, R. C., and D. C. Mountain. 1998. Measurements of the stiffness map challenge a basic tenet of cochlear theories. *Hear. Res.* 124: 124–131.
29. Cai, H. X., D. Manoussaki, and R. Chadwick. 2005. Effects of coiling on the micromechanics of the mammalian cochlea. *J. R. Soc. Interface.* 2:341–348.
30. Nowotny, M., and A. W. Gummer. 2006. Nanomechanics of the subtectorial space caused by electromechanics of cochlear outer hair cells. *Proc. Natl. Acad. Sci. USA.* 103:2120–2125.
31. Fleischer, M., R. Schmidt, and A. W. Gummer. 2010. Compliance profiles derived from a three-dimensional finite-element model of the basilar membrane. *J. Acoust. Soc. Am.* 127:2973–2991.

32. Choe, Y., M. O. Magnasco, and A. J. Hudspeth. 1998. A model for amplification of hair-bundle motion by cyclical binding of Ca^{2+} to mechanoelectrical-transduction channels. *Proc. Natl. Acad. Sci. USA.* 95:15321–15326.
33. Tinevez, J. Y., F. Jülicher, and P. Martin. 2007. Unifying the various incarnations of active hair-bundle motility by the vertebrate hair cell. *Biophys. J.* 93:4053–4067.
34. Tolomeo, J. A., and C. R. Steele. 1998. A dynamic model of outer hair cell motility including intracellular and extracellular fluid viscosity. *J. Acoust. Soc. Am.* 103:524–534.
35. Zheng, J. F., N. Deo, …, A. L. Nuttall. 2007. Chlorpromazine alters cochlear mechanics and amplification: in vivo evidence for a role of stiffness modulation in the organ of Corti. *J. Neurophysiol.* 97: 994–1004.
36. Iwasa, K. H. 2001. A two-state piezoelectric model for outer hair cell motility. *Biophys. J.* 81:2495–2506.
37. Salt, A. N., N. Inamura, …, A. Vora. 1989. Calcium gradients in inner ear endolymph. *Am. J. Otolaryngol.* 10:371–375.
38. Fridberger, A., A. Flock, …, B. Flock. 1998. Acoustic overstimulation increases outer hair cell Ca^{2+} concentrations and causes dynamic contractions of the hearing organ. *Proc. Natl. Acad. Sci. USA.* 95:7127–7132.
39. Cooper, N. P. 1998. Harmonic distortion on the basilar membrane in the basal turn of the guinea-pig cochlea. *J. Physiol.* 509:277–288.
40. He, D. Z. Z., S. P. Jia, and P. Dallos. 2004. Mechanoelectrical transduction of adult outer hair cells studied in a gerbil hemicochlea. *Nature.* 429:766–770.
41. Kössl, M., and I. J. Russell. 1992. The phase and magnitude of hair cell receptor potentials and frequency tuning in the guinea pig cochlea. *J. Neurosci.* 12:1575–1586.
42. Dallos, P. 1996. Overview: cochlear neurobiology. *In* The Cochlea. P. Dallos, A. N. Popper, and R. R. Fay, editors. Springer, New York. 1–43.
43. Russell, I. J., and M. Kössl. 1992. Voltage responses to tones of outer hair cells in the basal turn of the guinea-pig cochlea: significance for electromotility and desensitization. *Proc. Biol. Sci.* 247:97–105.
44. Fridberger, A., J. B. de Monvel, …, A. Nuttall. 2004. Organ of Corti potentials and the motion of the basilar membrane. *J. Neurosci.* 24:10057–10063.
45. Iwasa, K. H., and M. Adachi. 1997. Force generation in the outer hair cell of the cochlea. *Biophys. J.* 73:546–555.
46. Zwislocki, J. J., and E. J. Kletsky. 1979. Tectorial membrane: a possible effect on frequency analysis in the cochlea. *Science.* 204:639–641.
47. Gummer, A. W., W. Hemmert, and H. P. Zenner. 1996. Resonant tectorial membrane motion in the inner ear: its crucial role in frequency tuning. *Proc. Natl. Acad. Sci. USA.* 93:8727–8732.
48. Ospeck, M., X. X. Dong, and K. H. Iwasa. 2003. Limiting frequency of the cochlear amplifier based on electromotility of outer hair cells. *Biophys. J.* 84:739–749.
49. Kros, C. J., A. Rüsch, and G. P. Richardson. 1992. Mechano-electrical transducer currents in hair cells of the cultured neonatal mouse cochlea. *Proc. Biol. Sci.* 249:185–193.
50. van Netten, S. M., and C. J. Kros. 2000. Gating energies and forces of the mammalian hair cell transducer channel and related hair bundle mechanics. *Proc. Biol. Sci.* 267:1915–1923.
51. Nam, J. H., and R. Fettiplace. 2008. Theoretical conditions for high-frequency hair bundle oscillations in auditory hair cells. *Biophys. J.* 95:4948–4962.
52. Atkins, P., and J. de Paula. 2002. Atkin's Physical Chemistry. Oxford University Press, Oxford, UK.
53. Choudhury, N., G. Song, …, A. L. Nuttall. 2006. Low coherence interferometry of the cochlear partition. *Hear. Res.* 220:1–9.
54. Hong, S. S., and D. M. Freeman. 2006. Doppler optical coherence microscopy for studies of cochlear mechanics. *J. Biomed. Opt.* 11:054014.
55. Chan, D. K., and A. J. Hudspeth. 2005. Ca^{2+} current-driven nonlinear amplification by the mammalian cochlea in vitro. *Nat. Neurosci.* 8:149–155.